doi.org/10.26434/chemrxiv.9640862.v1

Supramolecular Enhancement of Aminoxyl ORCA Contrast Agents

Hamilton Lee, Jenica Lumata, Michael A. Luzuriaga, Candace Benjamin, Olivia Brohlin, Christopher R. Parish, Steven O. Nielsen, Lloyd Lumata, Jeremiah J. Gassensmith

Submitted date: 16/08/2019 • Posted date: 19/08/2019

Citation information: Lee, Hamilton; Lumata, Jenica; Luzuriaga, Michael A.; Benjamin, Candace; Brohlin, Olivia; Parish, Christopher R.; et al. (2019): Supramolecular Enhancement of Aminoxyl ORCA Contrast Agents. ChemRxiv. Preprint.

Many contrast agents for magnetic resonance imaging are based on gadolinium, however side effects limit their use in some patients. Organic radical contrast agents (ORCAs) are potential alternatives, but are reduced rapidly in physiological conditions and have low relaxivities as single molecule contrast agents. Herein, we use a supramolecular strategy where cucurbit[8]uril binds with nanomolar affinities to ORCAs and protects them against biological reductants to create a stable radical in vivo. We further over came the weak contrast by conjugating this complex on the surface of a self-assembled biomacromolecule derived from the tobacco mosaic virus.

File list (3)

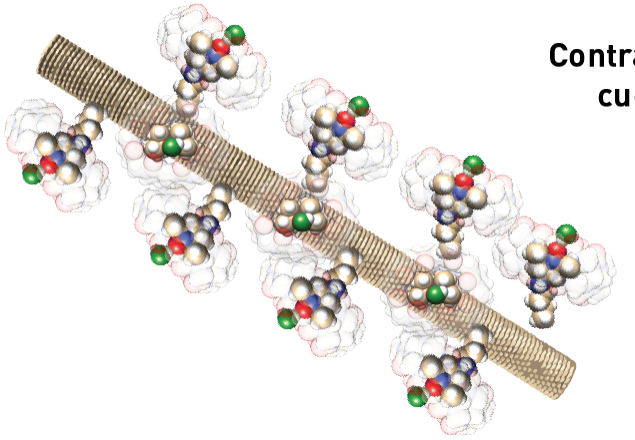

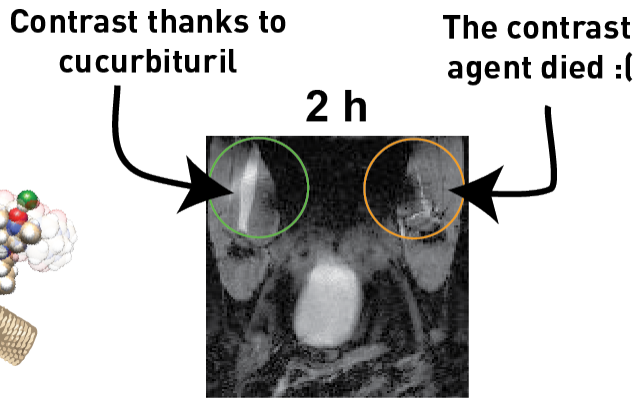
Contrast thanks to
cucurbituril
The contrast
agent died :(
2 h

Supramolecular Enhancement of Aminoxyl ORCA Contrast Agents

Hamilton Lee,[a] Jenica L. Lumata,[a] Michael A. Luzuriaga,[a] Candace E. Benjamin,[a] Olivia R. Brohlin,[a] Christopher R. Parish,[b] Steven O. Nielsen,[a] Lloyd L. Lumata [b] and Jeremiah J. Gassensmith [a, c] *

[a]Department of Chemistry and Biochemistry, [b]Department of Physics, [c]Department of Bioengineering, University of Texas at Dallas, Richardson, Texas 75080, United States

Contents

Materials

All chemicals were purchased from Sigma-Aldrich (St. Louis, MO), ThermoFisher Scientific (Pittsburgh, PA), Alfa Aesar (Ward Hill, MA), TCI America (Portland, OR), VWR International (Radnor, PA), and used without further purification.

Instrumentation

^{1}H and ^{13}C NMR spectra were obtained using a 600 MHz Bruker Avance NMR spectrometer with residual solvent peaks as a reference for all NMR spectra. Thiophenol (10-20 eq) were added to samples containing aminoxyl radicals to reduce them to hydroxylamines so that the compound could be observed via NMR. ESI-MS were acquired using a Agilent 1100 HPLC with a PLRP-S column for separation and an ABSciex 4000 QTRAP system for detection. Size exclusion chromatography (SEC) was conducted using an Agilent 1100 HPLC with a Phenomenex PolySep-GFC-P Linear 300 × 7.8 mm column. Isothermal titration calorimetry (ITC) was conducted using a Malvern Microcal iTC200. Transmission electron microscopy (TEM) was conducted using a JEOL JEM-1400Plus transmission electron microscope. Fluorescence data were obtained using a BioTek Synergy H4 Hybrid microplate reader. EPR spectroscopy was performed using a Bruker EMX ER041XG X-band spectrometer with a Bruker ER 4119HS resonator. NMR relaxometry experiments were performed with a 43 MHz Magritek Spinsolve NMR spectrometer operating with a magnetic field strength of 1 T.

Synthesis

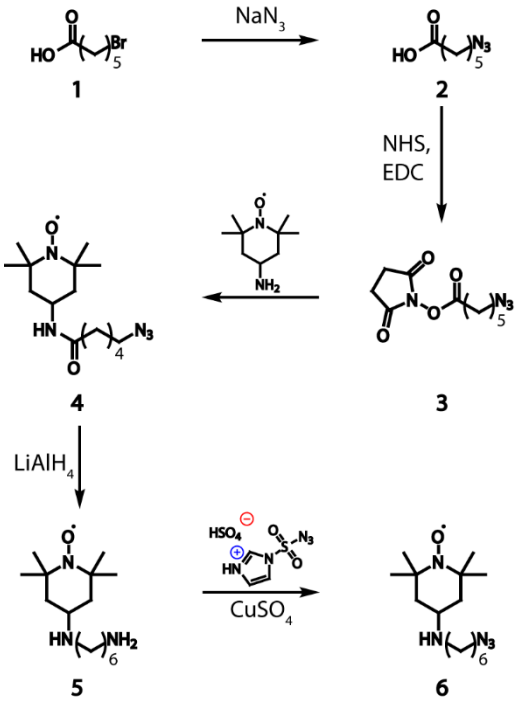

Scheme S1. Synthesis of **6**.

Synthesis of Imidazole-1-sulfonyl azide hydrogen sulfate

NaN_3 (10 g, 154 mmol) was stirred in dry EtOAc (150 mL) at 0 °C, 0.5 h. Sulfuryl chloride (20.7 g, 12.4 mL, 153 mmol) was added dropwise while stirring was maintained. The resulting mixture was stirred at RT, 24 h. The reaction mixture was cooled to 0 °C in an ice bath. Imidazole (20 g, 294 mmol) was slowly added over 5 min. The resulting mixture was stirred at 0 °C, 5 h. A saturated $NaHCO_3$ solution (aq.) (300 mL) was added to the reaction mixture. The organic fraction was isolated, washed with H_2O (3×100 mL) and dried with $MgSO_4$. The organic fraction was filtered and the filtrate was collected. The resulting solution was cooled to 0 °C in an ice bath while stirring was maintained. H_2SO_4 (18 M, 8.4 mL, 151 mmol) was added dropwise over 5 min while vigorous stirring was maintained. The resulting solution was stirred vigorously at RT until colorless or white precipitate was formed. The reaction mixture was filtered and the feed was washed with EtOAc (0 °C). The feed was collected and solvent was removed under reduced pressure to yield the product as a white solid. Yield: 35.3 g, 85 %. ^{1}H NMR (600 MHz, DMSO-*d*$_6$) δ ppm 7.67 (s, 1 H), 8.01 (s, 1 H), 9.06 (s, 1 H), 10.43 (s, 1 H), 14.28 (s, 1 H). ^{13}C NMR (150 MHz, DMSO-*d*$_6$) δ ppm 129.8, 134.4, 137.9.

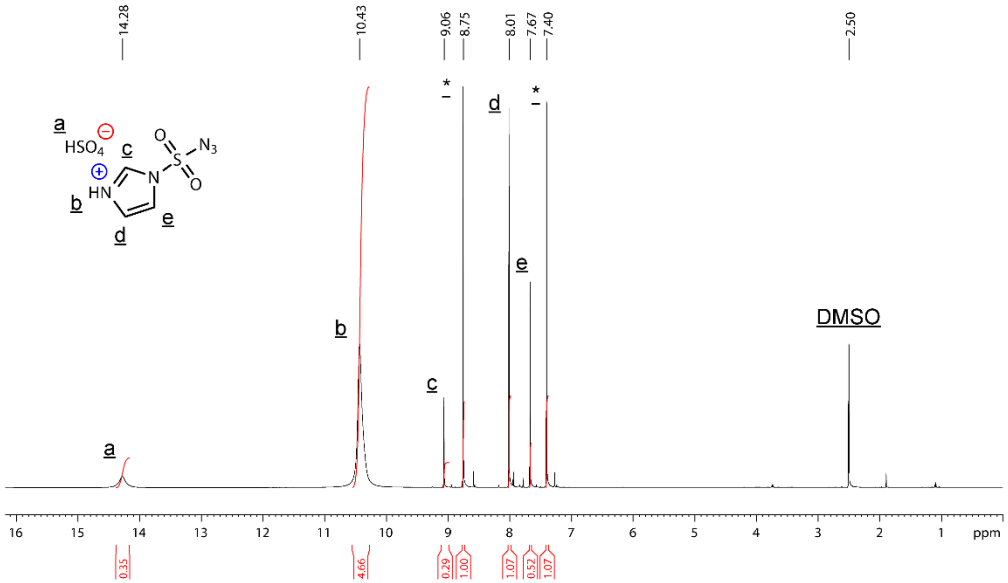

Figure S1. ^{1}H NMR spectrum of imidazole-1-sulfonyl azide hydrogen sulfate. Asterisks indicate decomposition products.

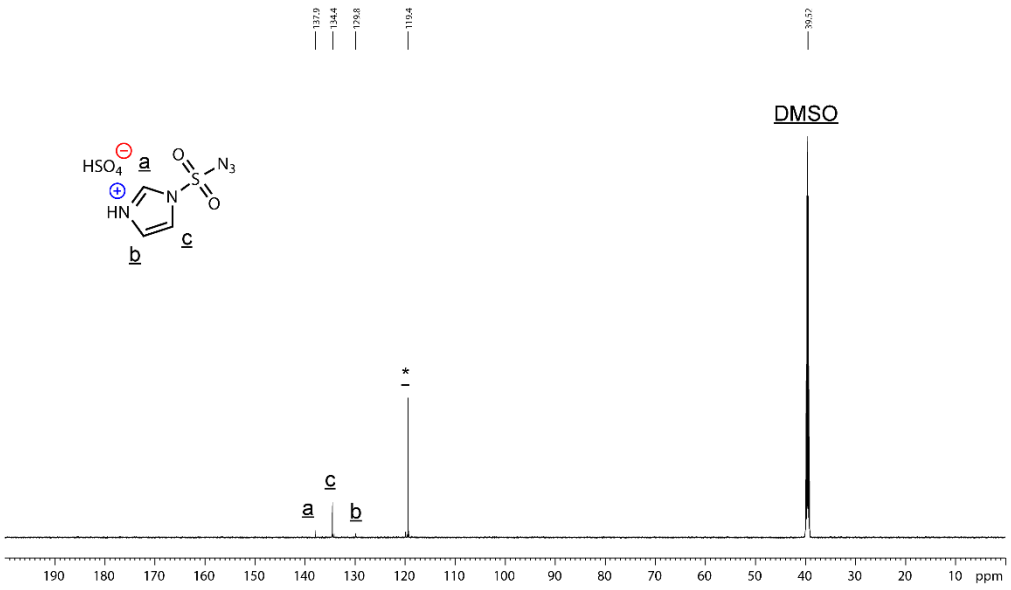

Figure S2. ^{13}C NMR spectrum of imidazole-1-sulfonyl azide hydrogen sulfate.

Synthesis of 6-Azidohexanoic acid **(2)**

Compound **1** (5.0 g, 25.6 mmol), and NaN_3 (4.998 g, 76.9 mmol) were stirred in DMF (20 mL) at 85 °C overnight. Upon cooling the reaction to RT, DCM (40 mL) was added to the reaction mixture and stirred. The reaction mixture was then washed with aqueous HCl (0.1 M, 3×20 mL) and dried with $MgSO_4$. The organic fraction was isolated and the solvent was removed under reduced pressure to yield the product as a clear pale yellow oil. Yield: 3.85 g, 96 %. ^{1}H NMR (600 MHz, $CDCl_3$) δ ppm 1.43 (quint, J = 7.2 Hz, 2 H), 1.61 (quint, J = 7.2 Hz, 2 H), 1.67 (t, J = 7.2 Hz, 2 H), 2.37 (quint, J = 7.2 Hz, 2 H), 3.27 (t, J = 6.4 Hz, 2 H).

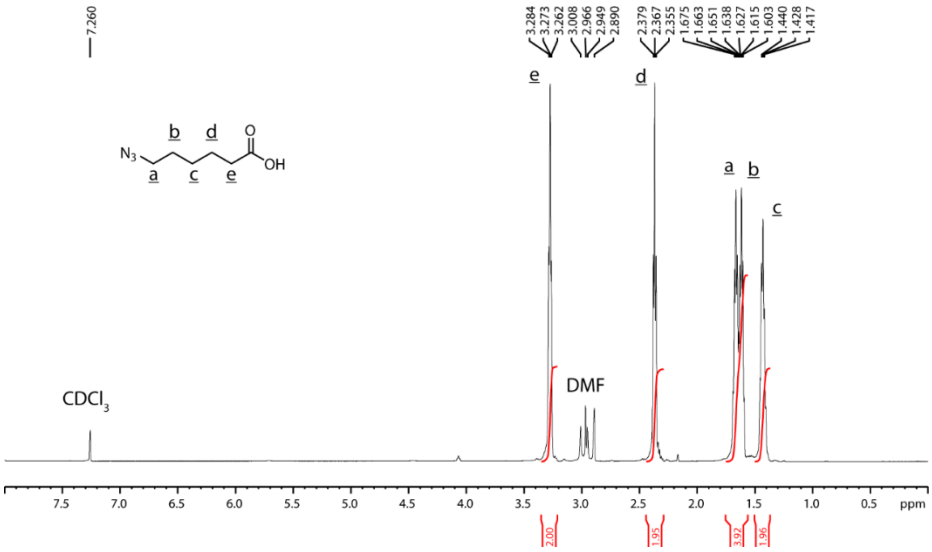

Figure S3. ^{1}H NMR spectrum of **2**.

Synthesis of 2,5-Dioxopyrrolidin-1-yl 6-azidohexanoate **(3)**

Compound **2** (2.0 g, 12.7 mmol), *N*-hydroxysuccinimide (NHS) (4.395 g, 38.2 mmol), and 1-ethyl-3-(3-dimethylaminopropyl)carbodiimide (EDC) (5.929 g, 38.2 mmol) were dissolved in DMF (15 mL) and stirred at RT, 48 h. DMF was then removed under reduced pressure. The remaining residue was dissolved in ethyl acetate (EtOAc) (25 mL). The organic layer was washed with H_2O (3×40 mL), saturated brine (3×40 mL), and dried with $MgSO_4$. The solvent was removed under reduced pressure to yield the crude product. The crude product was further purified via column chromatography (silica gel) with Hexanes:EtOAc (100:0-0:100). The fractions corresponding to the product were combined and the solvent was removed under reduced pressure to yield the product as a clear pale yellow oil. Yield: 2.80 g, 87 %. ^{1}H NMR (600 MHz, $CDCl_3$) δ ppm 1.49 (quint, J = 6.8 Hz, 2 H), 1.63 (quint, J = 7.1 Hz, 2 H), 1.77 (t, J = 7.0 Hz, 2 H), 2.61 (quint, J = 7.1 Hz, 2 H), 2.82 (s, 4 H), 3.28 (t, J = 6.4 Hz, 2 H).

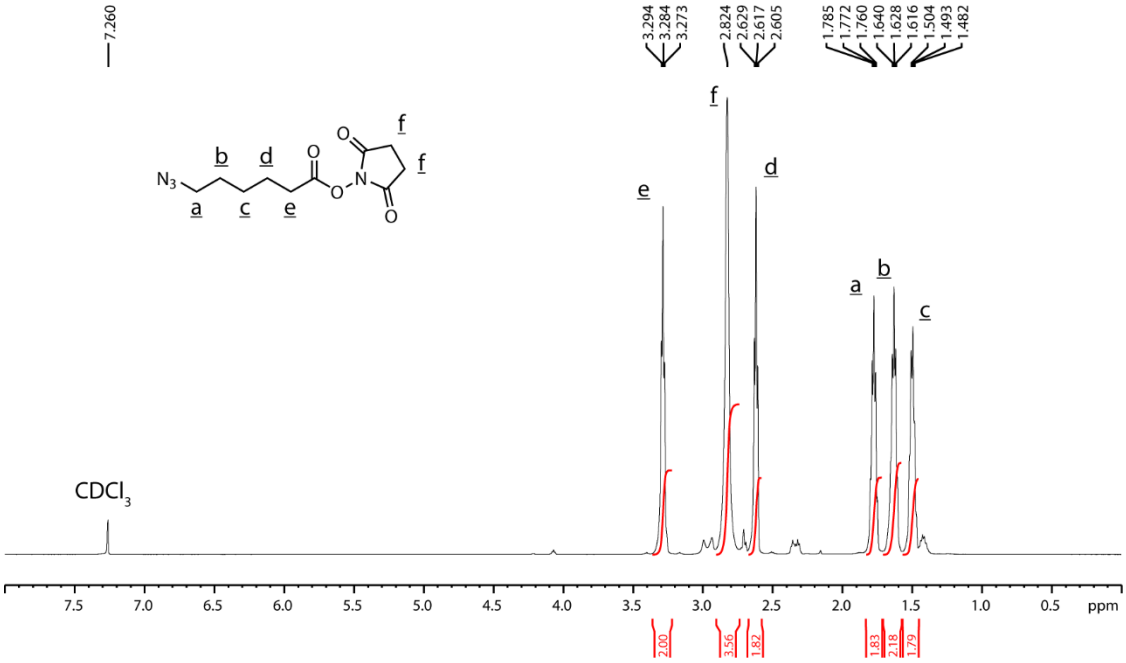

Figure S4. ^{1}H NMR spectrum of **3**.

Synthesis of 6-Azido-N-(1-oxyl-2,2,6,6-tetramethylpiperidin-4-yl)hexanamide (4)

4-Amino-2,2,6,6-tetramethylpiperidine-1-oxyl (2.0 g, 11.7 mmol), **3** (5.94 g, 23.3 mmol), and TEA (1.18 g, 11.7 mmol) were dissolved in dry (need not be anhydrous) DMF (25 mL). Potassium carbonate (1.61 g, 11.7 mmol) was added and the mixture was stirred at RT, OVN. DCM (50 mL) and H_2O (20 mL) were added and the reaction mixture was washed with H_2O (3×50 mL). The aqueous fraction was extracted with DCM (2×25 mL) and the organic fractions were combined. The organic fraction was washed with H_2O (3×50 mL) and dried with $MgSO_4$. The solvent was removed under reduced pressure. The crude product was further purified via column chromatography (silica) with DCM:MeOH (100:0 - 90:10). The solvent was removed under reduced pressure to yield the product as a red liquid. Yield: 6.52 g, 90 %. ^{1}H NMR (600 MHz, $CDCl_3$) δ ppm 0.90-2.30 (m, 26 H), 3.28 (t, 1 H). ^{13}C NMR (150 MHz, $CDCl_3$) δ ppm 19.83, 25.15, 25.20, 26.44, 28.73, 36.62, 41.21, 45.57, 51.35.

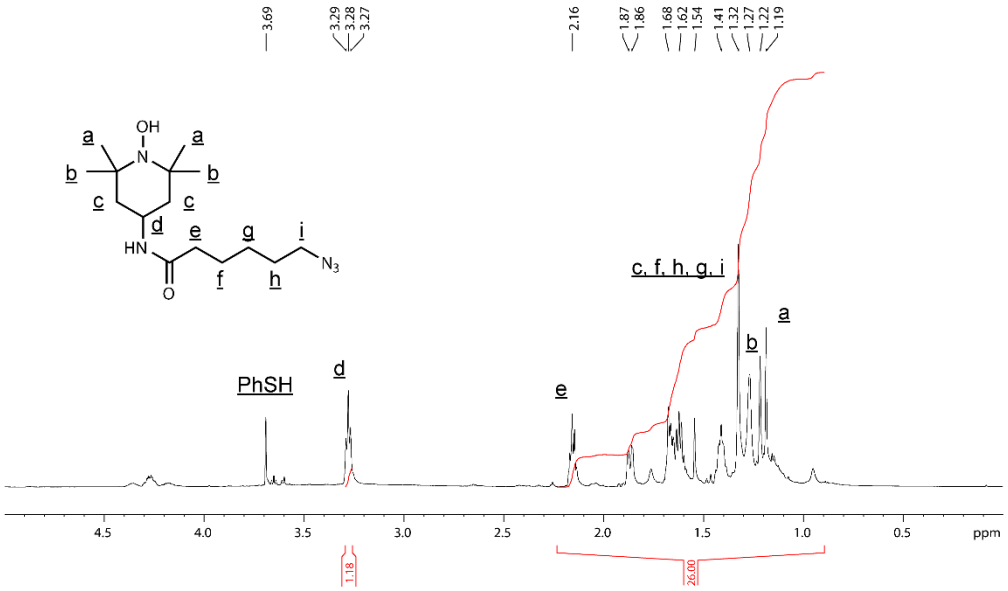

Figure S5. ^{1}H NMR spectrum of **4**.

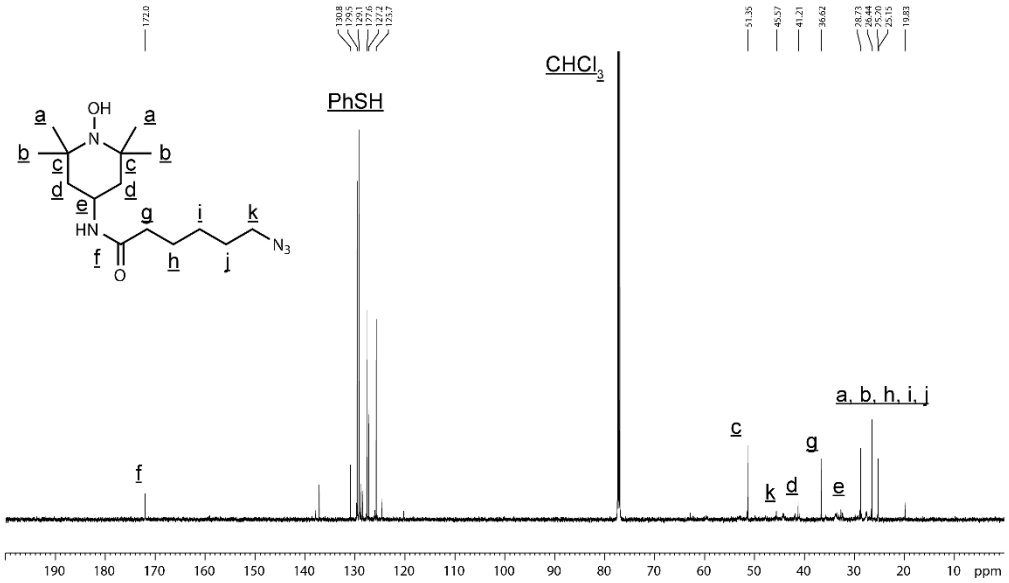

Figure S6. ^{13}C NMR spectrum of **4**.

Synthesis of 4-((6-Aminohexyl)amino)-2,2,6,6-tetramethylpiperidin-1-oxyl **(5)**

Compound **4** (2.0 g, 6.4 mmol) was dissolved in Et_2O (100 mL) and $LiAlH_4$ (2.45 g, 64 mmol) was slowly added portionwise to the reaction solution. The reaction mixture was stirred at RT, OVN. The reaction mixture was cooled to 4 °C in an ice bath. H_2O (1.22 mL), followed by an aqueous NaOH solution (15% w/v, 1.22 mL), followed by H_2O (3.66 mL) were slowly added to the reaction mixture under stirring. Stirring was continued for 15 min. The reaction mixture was dried with $MgSO_4$ and stirred for 15 min. The resulting mixture was filtered and the feed was washed with Et_2O (100 mL). The organic fractions were combined. The solvent was removed under reduced pressure. The crude product was further purified via column chromatography (alumina) with DCM:MeOH (100:0 - 90:10). The solvent was removed under reduced pressure to yield the product as a light orange liquid. The crude compound was used without further purification. Yield: 1.27 g, 73 %.

Synthesis of 4-((6-Azidohexyl)amino)-2,2,6,6-tetramethylpiperidin-1-oxyl **(6)**

Compound **5** (2.0 g, 7.4 mmol) was dissolved in MeOH (50 mL) and the reaction solution was cooled to 4 °C in an ice bath. 1*H*-Imidazole-1-sulfonyl azide hydrogen sulfate (2.21 g, 8.1 mmol), $CuSO_4 \cdot 5H_2O$ (0.02 g, 0.074 mmol), and K_2CO_3 (2.04 g, 14.8 mmol) were added and the reaction mixture was stirred at RT, OVN. The solvent was removed under reduced pressure. H_2O (25 mL) was added to the remaining residue and the resulting mixture was filtered. The feed was washed with H_2O (25 mL) and EtOAc (25 mL). The filtrate was collected and H_2O (25 mL) was added. The organic fraction was collected. The aqueous fraction was extracted w/ EtOAc (2×25 mL) and the organic fractions were combined. The combined organic fraction was washed with $NaHCO_3$ (aq.) (4% w/v, 2×30 mL), and saturated brine (2×30 mL). The organic fraction was collected and dried with $MgSO_4$. The solvent was removed under reduced pressure to yield the crude product. The crude product was further purified via column chromatography (alumina) with DCM:MeOH (100:0 - 90:10). The solvent was removed under reduced pressure to yield the product as a red liquid. Yield: 1.84 g, 84 %. ^{1}H NMR (600 MHz, $CDCl_3$) δ ppm 1.15-20 (m, 12 H), 1.41 (m, 4 H), 1.62 (m, 4 H), 1.87 (m, 4 H), 3.17 (m, 1 H), 3.27 (t, 2 H), 3.65 (t, 2 H). ^{13}C NMR (150 MHz, $CDCl_3$) δ ppm 20.45, 20.47, 25.21, 26.32, 27.76, 28.62, 36.29, 39.38, 42.80, 51.28, 67.32, 67.97.

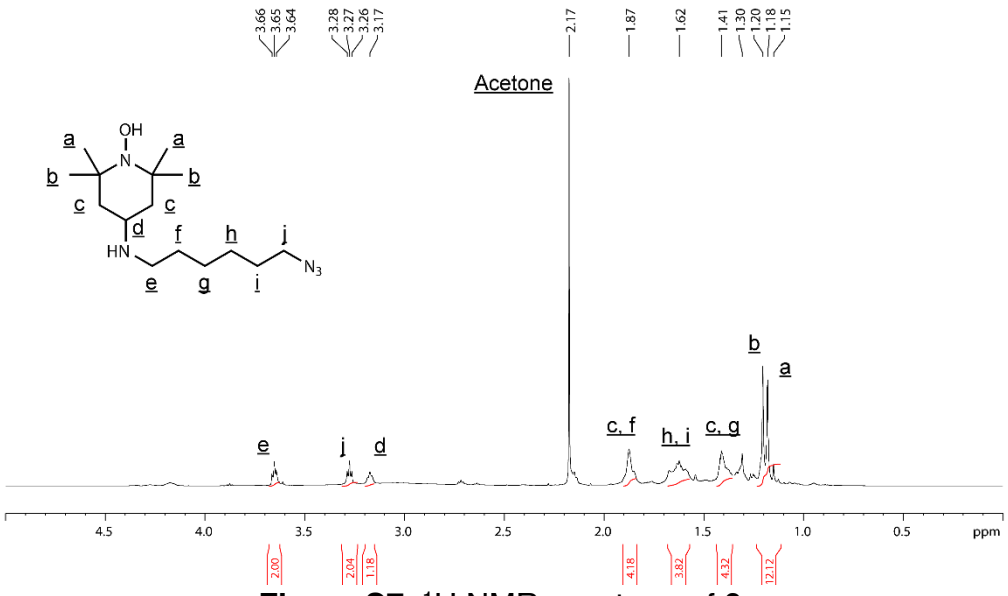

Figure S7. ^{1}H NMR spectrum of **6**.

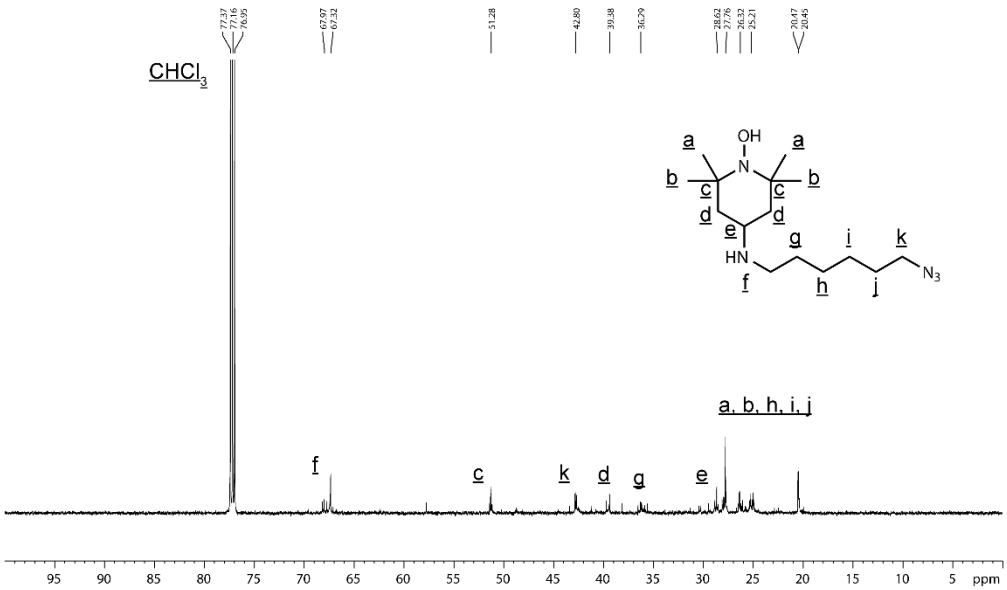

Figure S8. ^{13}C NMR spectrum of **6**.

Isothermal Titration Calorimetry

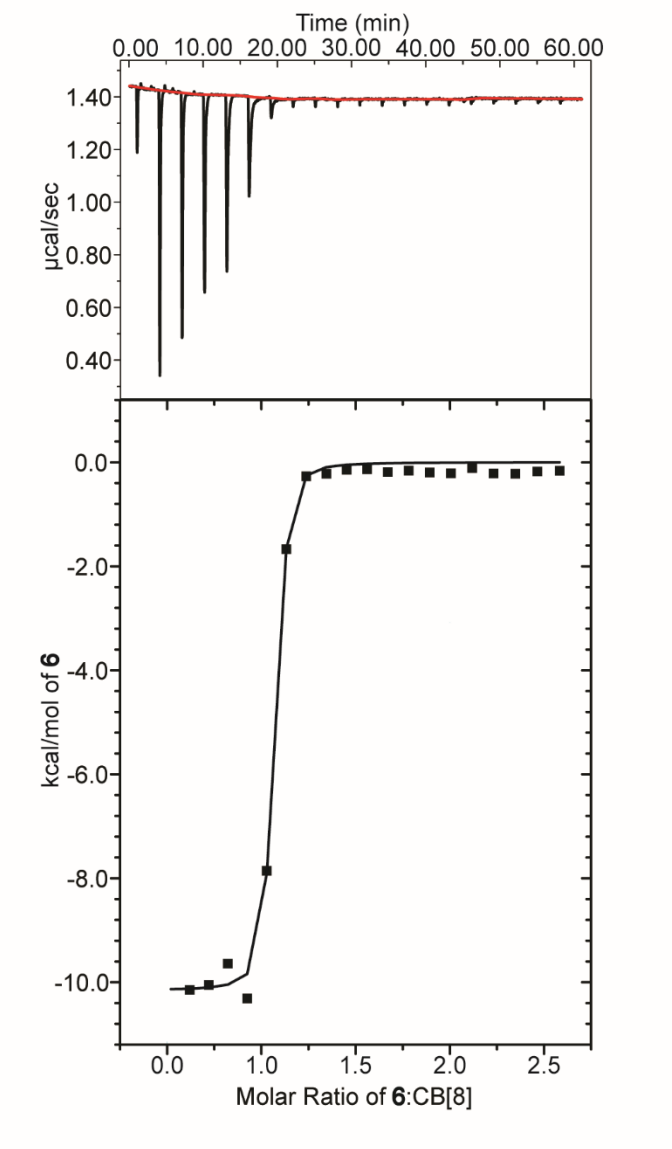

Figure S9. ITC data for **6** at 25 °C in 10 mM sodium phosphate (pH 7.0). **6** (250 µM) was titrated into a solution of CB[8] (50 µM). The top portion of the figure is a plot of power versus time. The bottom portion of the figure are integrated enthalpy values versus the molar ratio of **6**:CB[8]. The K_d value for the CB[8]⊃**6** complex was determined to be 1.5 ± 0.1 × 10^{-8} M. The enthalpy and entropy values were determined to be -1.0× 10^4 ± 118.2 cal/mol and 16.0 cal/mol/deg respectively. These data were fit to a one-binding site model using Origin 8.0 software.

Protocol for Expression of TMV

TMV particles were isolated from *Nicotiana benthamiana* plants. Tobacco plants were grown, infected with a solution of TMV from a stock source, collected (~10 d after infection), and stored at –80 °C until needed. The leaves (~100 g) were blended with cold (4 °C) extraction buffer (KP buffer (0.1 M, 1000 mL, pH 7.4) with 2-mercaptoethanol (0.2% (v/v))), followed by thorough grinding with a mortar and pestle. The mixture was filtered through cheesecloth to remove the plant solids, and the filtrate centrifuged at 11,000 ×*g* (4 °C, 20 min). The supernatant was filtered through cheesecloth again, and an equal volume of 1:1 chloroform/1-butanol mixture was added and stirred (4 °C, 30 min). The mixture was centrifuged at 4500 ×*g* for 10 min. The aqueous phase was collected, followed by the addition of NaCl (final concentration of 0.2 M), PEG 8000 (8% (w/w)), and Triton X-100 surfactant (1% (w/w)). The mixture was stirred on ice for 30 min and stored (4 °C, 1 h). The solution was centrifuged at 22,000 ×*g* (4 °C, 15 min). The supernatant was discarded, and the pellet resuspended in KP buffer (0.1 M, pH 7.4) (4 °C, OVN). The supernatant was carefully layered on a 40% (w/v) sucrose gradient (that had undergone at least one freeze-thaw cycle to create a moderate sucrose gradient) in KP buffer (0.01 M, pH 7.4) in ultracentrifuge tubes and centrifuged in a swing bucket rotor for 2 h at 96,000 ×*g*. An LED light positioned under the transparent centrifuge tube was used to illuminate the colloidal suspension, which appears blue from Mie scattering. The light-scattering region was collected and centrifuged at 360,562 ×*g* for 1.5 h. The supernatant was discarded, and the pellet resuspended in KP buffer (0.01 M, pH 7.4) (4 °C, OVN). The solution was portioned equally into microcentrifuge tubes and centrifuged at 15,513 ×*g* for 15 min. The supernatant was collected as the final TMV solution. UV-Vis measurements were taken at 260 nm (RNA) and 280 nm (protein). A ratio of A260/A280 around 1.23 indicates intact TMV. Using the Beer-Lambert Law with $\varepsilon = 3$ the concentration of the solution was determined.

Bioconjugation of TMV

Synthesis of TMV-Aky

Solutions of 3-ethynylaniline in acetonitrile (0.68 M, 75 µL) and $NaNO_2$ (aq.) (3.0 M, 25 µL) were added to a cold (4 °C) solution of p-toluenesulfonic acid (aq.) (0.3 M, 400 µL) and mixed well. The resulting solution was mixed in light-free conditions (4 °C, 1 h) to form the diazonium salt. A solution of TMV (20 mg/mL, 100 µL, 0.1 µmol) was diluted in borate buffer (0.1 M, pH 8.8, 862 µL) and the resulting solution was chilled to 4 °C. The diazonium salt solution (70 eq per coat protein of TMV, 76 µL) was added to the solution of TMV and the resulting solution was mixed in light-free conditions (4 °C, 45 min). The resulting product was purified via either size exclusion chromatography using a GE Healthcare PD-10 Desalting Column or centrifuge filtration using an EMD Millipore Amicon Ultra Centrifugal Filter Unit (10,000 MW Cutoff) (4,303 ×*g*).

*Synthesis of TMV-**6***

Compound **6** (1.7 mg, 5.7 μmol) was dissolved in DMSO (1 mL). Cold (4 °C) KP buffer (0.1 M, 3 mL, pH 7.4) was added to the resulting solution and mixed well. A cold (4 °C) solution of TMV-Aky (20 mg/mL, 100 μL, 0.1 μmol) in KP buffer (0.1 M, pH 7.4) was added to the resulting solution and mixed well. An aqueous solution of copper sulfate pentahydrate (0.1 M, 10 μL) was added to the resulting solution and mixed well. An aqueous solution of sodium ascorbate (0.2 M, 10 μL) was added to the resulting solution and mixed well. The reaction was left to proceed at RT for 24 h. The resulting product was purified via either size exclusion chromatography using a GE Healthcare PD-10 Desalting Column or centrifuge filtration using an EMD Millipore Amicon Ultra Centrifugal Filter Unit (10,000 MW Cutoff) (4,303 ×*g*).

Fluorescence and EPR Kinetics Experimental Details

Fluorescence titrations of TMV-**6** into CB[8]⊃PF were performed using Greiner 384-well, black, flat-bottomed plates. Solutions of TMV-**6** were prepared by serial dilutions of a stock solution of TMV-**6** (200 μM in terms of TEMPO) in sodium phosphate buffer (0.01 M, pH 7.0). TMV-**6**+CB[8]⊃PF solutions were prepared by mixing the appropriate TMV-**6** (20 μL) solution with the solution of CB[8]⊃PF (0.6 μM, 10 μL). This resulted in solutions with final TMV-**6** concentrations from 0-20 μM and a final CB[8]⊃PF concentration of 0.2 μM. The solutions were mixed by pipetting before reading the fluorescence intensities on the plate reader (top reading mode; 400 nm excitation, 10 nm bandwidth; 510 nm emission, 20 nm bandwidth). Z-depth and gain were optimized on the first scan and then exact values were used in subsequent scans. For the titrations of native TMV (nTMV) into CB[8]⊃PF, all methods and parameters were identical to the titrations of TMV-**6** into CB[8]⊃PF, except for the use of nTMV instead of TMV-**6**. For the titrations of TMV-**6** into PF, all methods and parameters were identical to the titrations of TMV-**6** into CB[8]⊃PF, except for the use of PF instead of CB[8]⊃PF.

Since no other significant interactions between TMV, **6**, CB[8], and PF were observed (**Figure S10, S11**) and assuming the conservation of mass, the relationship and equilibria of the titration components can be described by the following equation:

$$[\mathrm{CB[8]\cdot PF}]+[\mathbf{6}]\rightleftharpoons[\mathrm{CB[8]}]+[\mathrm{PF}]+[\mathbf{6}]\rightleftharpoons[\mathrm{CB[8]}\supset\mathbf{6}]+[\mathrm{PF}] \quad \text{(Eq. 1)}$$

Therefore, the two dissociation constants, K_a for the complex consisting of CB[8] and PF and K_b for the complex consisting of CB[8] and **6** can be represented by the following equations:

$$K_a=\frac{[\mathrm{CB[8]}][\mathrm{PF}]}{[\mathrm{CB[8]\cdot PF}]} \quad \text{(Eq. 2)}$$

$$K_b = \frac{[CB[8]][\mathbf{6}]}{[CB[8] \supset \mathbf{6}]} \quad \text{(Eq. 3)}$$

Equations 1-3 can then be combined to form the following cubic equation:

$$[CB[8]]^3 + a \cdot [CB[8]]^2 + b \cdot [CB[8]] + c = 0 \quad \text{(Eq. 4)}$$

where

$$a = K_a + K_b + [PF]_0 + [\mathbf{6}]_0 - [CB[8]]_0 \quad \text{(Eq. 5)}$$

$$b = K_b([PF]_0 - [CB[8]]_0) + K_a([\mathbf{6}]_0 - [CB[8]]_0) + K_a K_b \quad \text{(Eq. 6)}$$

$$c = -K_a K_b [CB[8]]_0 \quad \text{(Eq. 7)}$$

and $[PF]_0$, $[\mathbf{6}]_0$, and $[CB[8]]_0$ denote the total concentration of each respective compound. The change in the observed fluorescence intensity can be directly linked to the binding constants K_a and K_b by solving Equation 4 for the real root. The relationship between the observed fluorescence intensities and the binding constants are described by the equation:

$$F = F_{Min} + (F_{Max} - F_{Min}) \frac{2 \cdot \sqrt{(a^2 - 3b)} \cdot \cos\frac{\theta}{3} - a}{3K_a + \left[2 \cdot \sqrt{(a^2 - 3b)} \cdot \cos\frac{\theta}{3} - a\right]} \quad \text{(Eq. 8)}$$

where

$$\theta = \cos^{-1} \cdot \frac{-2a^3 + 9ab - 27c}{2 \cdot \sqrt{(a^2 - 3b)^3}} \quad \text{(Eq. 9)}$$

and F, F_{Min}, and F_{Max} denote the observed fluorescence intensity at any given point in the titration, the minimum observed fluorescence intensity during the titration, and the maximum observed fluorescence intensity during the titration, respectively. Upon fitting

Equation 8 to the observed fluorescence intensities, the K_d value for the CB[8]⊃TMV-**6** complex was determined to be 3.8 ± 0.5 × 10^{-7} M.

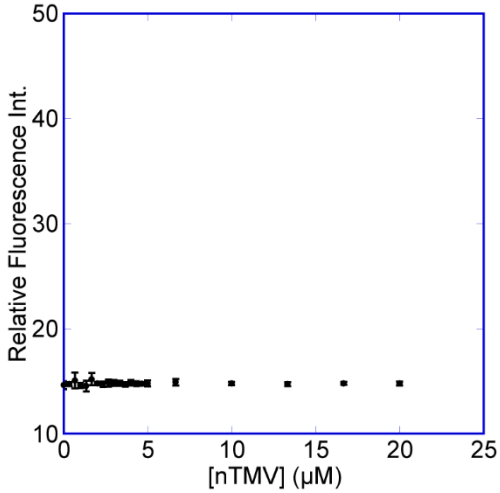

Figure S10. Fluorescence titration data for control experiment with nTMV and CB[8]⊃PF. nTMV (0-20 μM in terms of TMV coat protein) was titrated into solutions of CB[8]⊃PF (0.2 μM). Since no significant changes in fluorescence were observed, it is demonstrated that TMV does not compete with **6** to bind inside the cavity of CB[8].

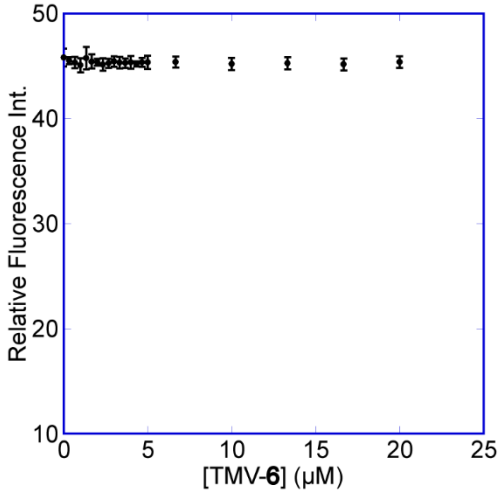

Figure S11. Fluorescence titration data for control experiement with TMV-**6** and PF. TMV-**6** (0-20 μM in terms of TEMPO) was titrated into solutions of PF (0.2 μM). Since no significant changes in fluorescence were observed, it is demonstrated that TMV does not quench the fluorescence of **6**.

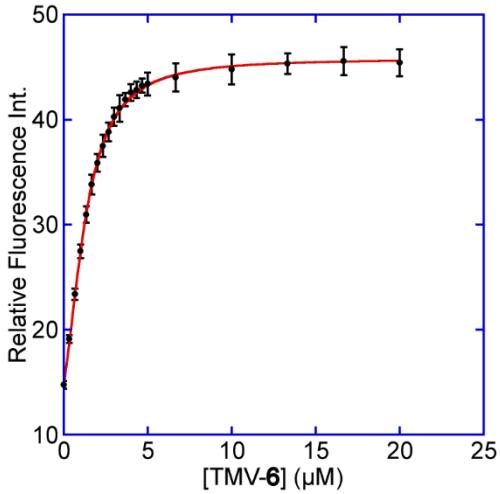

Figure S12. Fluorescence titration data for TMV-**6**. TMV-**6** (0-20 μM in terms of TEMPO) was titrated into solutions of CB[8]⊃PF (0.2 μM). The K_d value for the CB[8]⊃TMV-**6** complex was determined to be 3.8 ± 0.5 × 10^{-7} M.

EPR Spectroscopy

All EPR measurements were obtained using the following instrumental conditions:

-Microwave Power: 4.54 mW

-Microwave Frequency: 9.38 GHz

-Modulation Frequency: 100 kHz

-Modulation Amplitude: 0.4 mT (4 G)

-Temperature: 298 K

-Center Field: 334 mT (3340 G)

-Sweep Range: 8 mT (80 G)

Samples were prepared by filling a double-ended glass capillary tube (1 mm internal diameter) with the appropriate solution, sealing the capillary tube with paraffin laboratory film, and then placing the capillary tube in a quartz EPR tube (4 mm internal diameter).

Table S1: Kinetics of the reduction of nitroxides with excess of sodium ascorbate. Numerical fits to pseudo-first order rate equation (*k'*) for the relaxometric data of the reaction.

Agent	*Reduction with ascorbate k' (×10^{-5} s^{-1})*	Reference
TMV-6 with CB[8]	2.0	This work
exTEMPO-TMV,	170.0	**1**
TEMPO-conjugated branched-bottle brush polymer*	791.0	**2**
Chex-MIM*	37.9	**3**
P1*	27.0	**3**
Dendrimer*	57.8	**4**
TEMPOL*	633.3	**5**

*Determined with the integrated peak height (IPH) EPR data and for the initial kinetic fit (<1 hour).

MRI *In Vivo* Studies

All animal procedures were reviewed by the UT Southwestern IACUC committee and accepted under protocol # 2016-101780. Mice were placed under anesthesia and a heater was used to keep the temperature around the mice at 30 °C for the duration of the study. Each mouse was injected intramuscularly with 50 µL of TMV-6 without CB and TMV-6 with CB. The mice were placed in a 9.4 T Varian MRI scanner and the bladder was positioned to be in the center. 3D T1-weighted gradient echo multi slice scans were taken before injection (*TE* = 4.00 ms and *TR* = 256.92 ms, Matrix = 128 × 138 × 128) and at 1 min, 30 min, and 2 h after injection.

Modeling

The molecular dynamics (MD) simulations included one TEMPO molecule, one CB[8] molecule, 1877 water molecules, and one chloride anion in the unit cell under periodic boundary conditions. The force field parameters for CB[8] were obtained from CGenFF[6,

[7] using the online server at https://cgenff.paramchem.org. The force field parameters for TEMPO were obtained from the SLH moiety in work by Sezer *et al.*[8] The TIP3P water model was used. Note that the TIP3P water model was found to yield better agreement with experimental cucurbituril-guest binding enthalpies than competing water models such as TIP4P-Ew.[9]

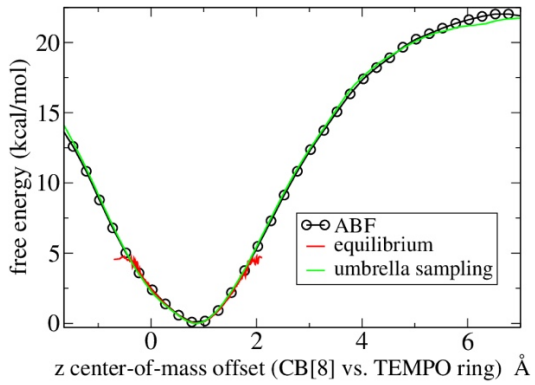

Figure S13. The free energy profile as a function of the insertion depth of the TEMPO ring in the CB[8] cavity.

All simulations were run using the NAMD software package[10] with the following parameter choices: temperature 300 K enforced with a Langevin thermostat with damping parameter 1.0 ps^{-1}; pressure 1 atm enforced with a Langevin barostat with a period of 100 fs and a decay time of 50 fs; cutoff distance 12 Å for the van der Waals interactions and the changeover from real space to reciprocal space for the electrostatic interactions; time step 1.0 fs; particle mesh Ewald grid spacing of 1 Å.

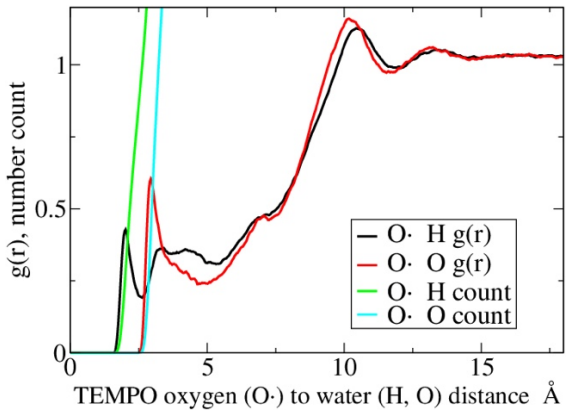

Figure S14. Radial distribution functions and their integrals for the distance between the TEMPO oxygen radical and water hydrogen and oxygen atoms.

Three simulations were run, namely an equilibrium simulation of 100 ns, an adaptive biasing force simulation of 100 ns, and an umbrella sampling simulation of 100 ns. The equilibrium simulation quantifies, among other things, the accessibility of the TEMPO oxygen radical to solvent water molecules. This data is shown in Fig. S14. We see that water hydrogen atoms (black line) are found preferentially about 2 Angstroms from the TEMPO oxygen radical, and water oxygen atoms (red line) are found preferentially about 3 Angstroms from the TEMPO oxygen radical. In terms of numbers, the green and blue curves in Fig. S14 show that, on average, one water hydrogen and one water oxygen are found within 2.6 and 3.2 Angstroms, respectively, of the TEMPO oxygen radical. A water molecule including this hydrogen and oxygen atom is shown in Fig. S15. This water molecule is surrounded by other solvent water molecules, thus allowing exchange to generate the MRI contrast. In addition, due to the CB[8] cavity, we see that the radial distribution functions do not plateau until about 15 Angstroms.

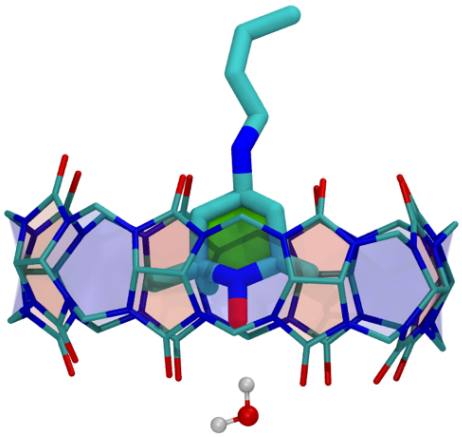

Figure S15. Representative snapshot from the equilibrium MD simulation showing the location of the TEMPO molecule with respect to CB[8] and the TEMPO oxygen radical's access to solvent water. Only one solvent water molecule is shown.

The two free energy simulations quantify the CB[8]—TEMPO host—guest binding free energy and also show exactly where the TEMPO molecule prefers to sit in the CB[8] host cavity. The data is shown in Fig. S13. We can notice two main observations. First, the equilibrium position of the TEMPO ring is about 0.9 Å above the plane of the CB[8] ring. Second, the binding free energy is very strong at over 20 kcal/mol. Previous literature suggests that computational methods typically overestimate the binding free energy for cucurbit[n]uril host-guest systems[11] but nonetheless the CB[8]—TEMPO association is clearly very strong.

Although we do not attempt to decompose the binding free energy into contributions from separate factors, we note that previous studies have attributed significant effects from the

change in solvation of the ammonium unit upon binding,[12] and from the release of water molecules inside the CB[8] cavity upon binding.[13]

For the binding free energy calculation, we used five collective variables to control the insertion of TEMPO into the CB[8] cavity and ensure reversibility of the transformation. The first two collective variables have no effect on the energy, the 3rd and 4th ones do have a minor effect on the energy, and the 5th one is the reaction coordinate. The 1st collective variable constrains the center of mass of CB[8] to the origin. The 2nd collective variable constrains the plane of the CB[8] ring to the x-y axis. These two collective variables have no effect on the system properties since periodic boundary conditions are used; their purpose is to make the choice of reaction coordinate simpler. The 3rd collective variable weakly constrains the center of mass of the TEMPO ring to the z-axis. This is done so that the TEMPO molecule does not drift sideways when it is separated from CB[8]. The 4th collective variable does not allow the terminal carbon atom in the TEMPO tail chain to be more than 3 Å below the center of mass of the TEMPO ring. This is done to prevent the TEMPO molecule from rotating 180 degrees which would otherwise potentially let it insert backwards after being separated from CB[8]. Although the entropic cost of the 3rd and 4th collective variable constraints could be estimated analytically, we simply neglected their contribution to the binding free energy. The 5th collective variable is defined as the z-distance between the center of mass of CB[8] and the center of mass of the TEMPO ring. This is our reaction coordinate for measuring the binding free energy. For the umbrella sampling run, it was controlled using 40 umbrellas between reaction coordinate values of -3 and +8 with a spring constant of 10 kcal/mol/Å^2 over a 100 ns simulation. For the ABF run we used the default values. We also computed the binding free energy, or at least the accessible portion, from the equilibrium simulation. This was done by taking kT times the negative of the logarithm of the normalized histogram of the reaction coordinate values visited during the equilibrium simulation.

References

1. M. Dharmarwardana, A. F. Martins, Z. Chen, P. M. Palacios, C. M. Nowak, R. P. Welch, S. Li, M. A. Luzuriaga, L. Bleris, B. S. Pierce, A. D. Sherry and J. J. Gassensmith, *Molecular Pharmaceutics*, 2018, **15**, 2973-2983.
2. A. O. Burts, Y. Li, A. V. Zhukhovitskiy, P. R. Patel, R. H. Grubbs, M. F. Ottaviani, N. J. Turro and J. A. Johnson, *Macromolecules*, 2012, **45**, 8310-8318.
3. M. A. Sowers, J. R. McCombs, Y. Wang, J. T. Paletta, S. W. Morton, E. C. Dreaden, M. D. Boska, M. F. Ottaviani, P. T. Hammond, A. Rajca and J. A. Johnson, *Nature Communications*, 2014, **5**, 5460.
4. A. Rajca, Y. Wang, M. Boska, J. T. Paletta, A. Olankitwanit, M. A. Swanson, D. G. Mitchell, S. S. Eaton, G. R. Eaton and S. Rajca, *Journal of the American Chemical Society*, 2012, **134**, 15724-15727.
5. J. T. Paletta, M. Pink, B. Foley, S. Rajca and A. Rajca, *Organic Letters*, 2012, **14**, 5322-5325.

6. K. Vanommeslaeghe and A. D. MacKerell, *Journal of Chemical Information and Modeling*, 2012, **52**, 3144-3154.
7. K. Vanommeslaeghe, E. P. Raman and A. D. MacKerell, *Journal of Chemical Information and Modeling*, 2012, **52**, 3155-3168.
8. D. Sezer, J. H. Freed and B. Roux, *The Journal of Physical Chemistry B*, 2008, **112**, 5755-5767.
9. A. T. Fenley, N. M. Henriksen, H. S. Muddana and M. K. Gilson, *Journal of Chemical Theory and Computation*, 2014, **10**, 4069-4078.
10. J. C. Phillips, R. Braun, W. Wang, J. Gumbart, E. Tajkhorshid, E. Villa, C. Chipot, R. D. Skeel, L. Kalé and K. Schulten, *Journal of Computational Chemistry*, 2005, **26**, 1781-1802.
11. J. I. Monroe and M. R. Shirts, *Journal of Computer-Aided Molecular Design*, 2014, **28**, 401-415.
12. X. Ling, S. Saretz, L. Xiao, J. Francescon and E. Masson, *Chemical Science*, 2016, **7**, 3569-3573.
13. F. Biedermann, M. Vendruscolo, O. A. Scherman, A. De Simone and W. M. Nau, *Journal of the American Chemical Society*, 2013, **135**, 14879-14888.

Other files

MS GM.pdf (574.42 KiB) view on ChemRxiv • download file